where $\langle r^2 \rangle$ is the average square radius of a particle in the state $|nljm\rangle$. For $j > 1/2$, the quadrupole moments turn out to be negative, that is, the probability distribution looks like a pancake in the plane perpendicular to the z-axis. For holes we have the opposite (i.e., prolate probability distributions). In Fig. 2.18, we see that this picture is qualitatively right in the neighborhood of magic numbers. However, as one fills the next shell with more and more nucleons, we soon find experimentally a transition to positive quadrupole moments with very large values. We shall see in the next chapter that in this case the average field of the nucleons is no longer spherical and we obtain a deformed density distribution. Only at the end of the shell, when nearly all levels are occupied, does one again get the picture of one or a few holes in a spherical core.

Even for one-particle or one-hole states with a magic core, this picture only gives qualitative agreement. Quantitatively, the measured quadrupole moments for proton states are roughly a factor of two larger than one would expect from (2.70) and values for neutron states do not vanish as they should according to Eq. (2.70), but behave as if the neutron had a charge. One usually expresses this fact by an effective charge e^{eff}. These effective charges can be explained by the polarization effect (see Sec. 9.3). Experimentally, it is observed that $e^{\text{eff}} \simeq 1$ for neutrons and $e^{\text{eff}} \simeq 2$ for protons.

The electric transitions behave very much like the corresponding moments. Only for the single-particle and single-hole nuclei near closed shells do they have values predicted by the single-particle shell model, with roughly the same effective charge as determined from the quadrupole moments.

Levels with *high angular momenta near closed shell* nuclei are often a mixture of only very few configurations (often there is only one configuration possible in a wide energy range). Sometimes—because of the selection rules of spin and parity—they can decay only by radiation with a high multipolarity. From Appendix B we learn that such transitions are highly suppressed because of kinematical factors. We therefore expect a very long lifetime for such nuclei. In fact, quite a few such "isomeric" states have been found in spherical nuclei (islands of isomers; see also Sec. 3.4.7).

2.8 Deformed Shell Model

2.8.1 Experimental Evidence

The assumption of approximately independent motion of nucleons in an average field is the basis of the shell model and of all microscopic theories of finite nuclei. This container potential is produced by the nucleons themselves and their mutual interaction. In Chapter 5 we shall see how to calculate this average potential. In its most simple form the potential well is spherical. This is true for nuclei with closed or nearly closed shells and, as we have seen in the last section, for such nuclei the spherical shell model

is very successful. Far from closed shells—that is, for mass numbers $A \simeq 25$ (Al, Mg), $150 < A < 190$ (nuclei of the rare earths) and for $A > 220$ (the actinides)—the independent particle picture again works quite well. However, in these regions one has to assume a deformed single particle potential. [Ra 50, 76, Bo 51].

The assumption of a deformation is able to explain many experimental facts, of which the most important are:

(i) **The existence of rotational bands.** In the mass regions mentioned above, the nuclear excitation spectra show pronounced rotational bands with an $I(I+1)$ spectrum, as in Eq. (1.64) (see, for instance, [BM 75]). As discussed in Chapter 1.5, such collective rotational bands are closely related to stable nuclear deformations.

(ii) **Very large quadrupole moments.** We have already seen in Section 2.7 that the spherical single-particle model with an inert core is by no means able to explain the large quadrupole moments in the regions far from closed shells (Fig. 2.18). This experimental fact is a hint about stable nuclear deformations, where the core also contributes to the quadrupole moment. Using the Bohr model [Eq. (1.75)] we can determine from the experimental (spectroscopic) quadrupole moment Q an intrinsic value Q_0, and derive a deformation parameter β [Eqs. (1.13) and (1.72)]. The "experimental" values of β, determined in this way, are for axial symmetric nuclei ($\gamma = 0$) in the rare earth region around

$$\beta \simeq 0.2\text{–}0.3. \tag{2.71}$$

The sign is positive. This means that we have cigar-shaped or prolate deformations. In other regions (for instance, $A \sim 25$, $A \sim 150$ or $A \sim 185$–190) there also exist pancake-shaped or oblate nuclei. Whether there also exist triaxial nuclei is still open to question (see Secs. 1.5.3 and 3.3.3).

(iii) **Strongly enhanced quadrupole transition probabilities.** In the rotational model, the quadrupole transition probabilities are directly connected to the intrinsic quadrupole moment Q_0 [see Eq. (1.73)]. The strongly enhanced BE2-values within the rotational bands are, therefore, another indication of stable quadrupole deformations.

(iv) **Hexadecupole matrix elements.** In (α, α') scattering [HGH 68] and Coulomb excitation, extremely large hexadecupole matrix elements have been found. This is a hint about stable hexadecupole deformations β_4. They are positive (diamond shaped figures; see Fig. 1.3) at the beginning, go to zero in the middle, and turn slightly negative at the end of the rare earth region.

(v) **Single particle structure.** A very sensitive experimental test for the deformation comes about from the experimentally observed single-particle energies, which depend very much on the details of the deformation (see Fig. 2.21).

(vi) **Fission isomers.** In some of the heaviest nuclei are found long

lived states (shape isomers $\tau \lesssim 1$ msec) that have extremely large deformations ($\beta \sim 0.6$) [PDK 62, St 66, Va 77]. The corresponding rotational spectra have been measured [SWK 72, Sp 74] and we can deduce the corresponding moments of inertia. It is clear that such large deformations play an important role in nuclear fission, and the deformed shell model will therefore also be of importance for this process.

Microscopic Hartree–Fock calculations in this region result in a deformed average potential and are indeed able to explain quantitatively the experimental findings (see Chap. 7). Conceptually, the deformed shell model is more involved than the spherical one, since in the formulation of the former we have to accept another symmetry violation—that of rotational invariance.

2.8.2 General Deformed Potential

If we accept the arguments given in Section 2.8.1 about stable nuclear deformation, we are naturally led to the assumption that the average nuclear potential is also deformed. Since the nuclear forces have a small range (~ 1 fm) compared to the nuclear diameter, one expects that the shape of this potential will be similar to the shape of the nuclear density distribution (which can be determined at least in principle from experimental data, e.g., the quadrupole or higher multipole moments). As we have already seen in the case of the spherical shell model, the Woods–Saxon potential (Eq. (2.4)) represents quite a good average potential. It is thus natural to generalize it to the deformed case* [FS 66, DPP 69, GPA 71]

$$V(r,\theta,\phi) = -V_0\left[1+\exp\left(\frac{r-R(\theta,\phi)}{a(\theta,\phi)}\right)\right]^{-1}. \tag{2.72}$$

In the spherical case, the parameter a describes the surface diffuseness and is approximately constant over all spherical nuclei, and therefore does not depend on the curvature of the surface. To get such a constant surface diffuseness for deformed nuclei also, one has to allow for a small dependence of $a(\theta,\phi)$ on the angles θ,ϕ (for more details, see [BM 75] and [BDJ 72]).

As we have seen in Section 2.4, the spin orbit term plays a very important role for the explanation of the level structure of spherical nuclei. In the deformed region, we also have to take it into account and a straightforward generalization of Eq. (2.18) is given by

$$V_{LS} = \lambda(\nabla V(r,\theta,\phi) \wedge \mathbf{p})\mathbf{s}. \tag{2.73}$$

This definition coincides with the one for the spherical case.

*For single-particle energies and wave functions of rare earth nuclei in a deformed Woods–Saxon potential, see [GIS 73].

As in the case of the spherical Woods–Saxon potential, another useful approximation to the general potential (2.72) and (2.73) is the harmonic oscillator, which has then, of course, to be deformed. This study, which we shall discuss now, was orginally carried out by S. G. Nilsson [Ni 55].

2.8.3 The Anisotropic Harmonic Oscillator

If we suppose for the moment that the density of a deformed nucleus can be ideally represented by an ellipsoidal distribution, then it follows from what has been said above that the average potential should also be ellipsoidal. In the harmonic oscillator approximation to the potential (2.72), this is most easily achieved by using the anisotropic harmonic oscillator as average field:

$$h_0 = -\frac{\hbar^2}{2m}\Delta + \frac{m}{2}\left(\omega_x^2 x^2 + \omega_y^2 y^2 + \omega_z^2 z^2\right). \tag{2.74}$$

The three frequencies $\omega_x, \omega_y, \omega_z$ have to be chosen proportional to the inverse of the half axes a_x, a_y, a_z of the ellipsoid:

$$\omega_\nu = \mathring{\omega}_0 \frac{R_0}{a_\nu}, \qquad (\nu = x, y, z). \tag{2.75}$$

The condition for volume conservation is, therefore,

$$\omega_x \omega_y \omega_z = \text{const.} = \mathring{\omega}_0^3. \tag{2.76}$$

The Hamiltonian (2.74) is separable in x, y, z. The eigenstates are characterized by the quantum numbers n_x, n_y, n_z, and the eigenvalues are:

$$\epsilon_0(n_x, n_y, n_z) = \hbar\omega_x\left(n_x + \tfrac{1}{2}\right) + \hbar\omega_y\left(n_y + \tfrac{1}{2}\right) + \hbar\omega_z\left(n_z + \tfrac{1}{2}\right). \tag{2.77}$$

In the case of *axially symmetric shapes*, one usually chooses the z-axis as symmetry axis and introduces a deformation parameter δ by the following definition:

$$\begin{aligned} \omega_\perp^2 = \omega_x^2 = \omega_y^2 &=: \omega_0^2(\delta)\left(1 + \tfrac{2}{3}\delta\right), \\ \omega_z^2 &=: \omega_0^2(\delta)\left(1 - \tfrac{4}{3}\delta\right), \end{aligned} \tag{2.78}$$

where δ is the only deformation parameter in this case, since $\omega_0(\delta)$ is determined in such a way that volume conservation is guaranteed. Up to quadratic terms in δ, we get from Eq. (2.76),

$$\omega_0(\delta) = \mathring{\omega}_0\left(1 + \tfrac{2}{3}\delta^2\right). \tag{2.79}$$

Nilsson therefore introduced a deformation-dependent oscillator length $b(\delta) = (\hbar/m\omega_0(\delta))^{1/2}$ and dimensionless coordinates $\mathbf{r}' = \mathbf{r}/b$. In these coordinates the Hamiltonian (2.74) has the form

$$h_0(\delta) = \hbar\omega_0(\delta)\left(-\frac{1}{2}\Delta' + \frac{1}{2}r'^2 - \frac{1}{3}\sqrt{\frac{16\pi}{5}}\,\delta r'^2 Y_{20}(\theta', \phi')\right). \tag{2.80}$$

The equipotential surfaces are ellipsoids. In first order in the deformation δ they can be represented by Eq. (1.7).

$$r' \sim (1 + \beta Y_{20}(\theta', \phi')), \tag{2.81}$$

with

$$\beta = \frac{1}{3}\sqrt{\frac{16\pi}{5}}\,\delta + \cdots = 1.057\delta + \cdots. \tag{2.82}$$

The deformation parameter δ of Eq. (2.78) is therefore roughly equal to β [Eq. (1.13)].

In the case of axial symmetry, it is convenient to use cylinder coordinates [Fl 71]. The eigenstates are characterized by quantum numbers n_z, n_ρ, m_l, where m_l is the projection of the orbital angular momentum on to the symmetry axis. With

$$N = n_z + 2n_\rho + m_l = n_x + n_y + n_z, \tag{2.83}$$

we get from Eq. (2.77)

$$\epsilon_0(n_z, n_\rho, m_l) = \hbar\omega_z\left(n_z + \tfrac{1}{2}\right) + \hbar\omega_\perp(2n_\rho + m_l + 1) \tag{2.84}$$

$$\simeq \hbar\dot{\omega}_0\left\{\left(N + \frac{3}{2}\right) + \delta\left(\frac{N}{3} - n_z\right)\right\}. \tag{2.85}$$

The axial symmetry causes m_l to be a good quantum number. The same is true for the spin component s_z and the z-component j_z of the total angular momentum, which has the eigenvalue

$$\Omega = m_l + m_s = m_l \pm \tfrac{1}{2}. \tag{2.86}$$

It is usual to characterize the eigenstates of h_0 in the cylindrical basis by the set of "Nilsson" quantum numbers

$$\Omega\pi[Nn_z m_l], \tag{2.87}$$

where π is the parity of the states [$\pi = (-1)^l = (-1)^N$; see Eq. (2.9)].

To discuss the level structure for a definite example, we use $N = 3$. From Eq. (2.85), we obtain in this case

$$\epsilon_0^{N=3}(n_z n_\rho m_l) \simeq \frac{9}{2}\hbar\dot{\omega}_0 + \hbar\dot{\omega}_0\delta(1 - n_z). \tag{2.88}$$

Table 2.2 Construction of the Nilsson quantum numbers for $N = 3$

n_z	m_l	n_ρ	Ω	degeneracy
0	1 3	1 0	1/2 3/2 5/2 7/2	4-fold
1	0 2	1 0	1/2 3/2 5/2	3-fold
2	1	0	1/2 3/2	2-fold
3	0	0	1/2	1-fold

Using Eqs. (2.83) and (2.86), we get the following possjbilities for the different quantum numbers, which are displayed in Table 2.2.

According to Eqs. (2.85) and (2.88), the levels with different values of n_z are split for small deformations proportionally to δ. This is shown in Fig. 2.19.

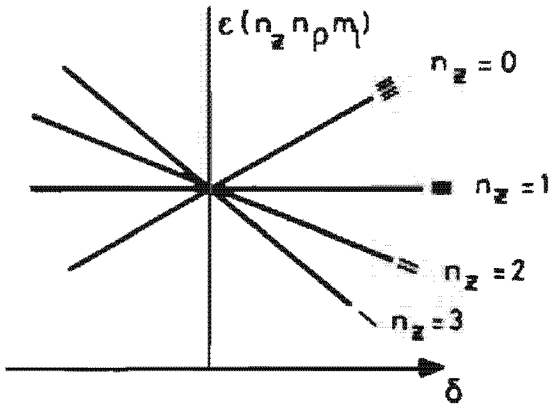

Figure 2.19. Levels of the anisotropic harmonic oscillator as a function of δ.

2.8.4 Nilsson Hamiltonian

As we have seen in Sec. 2.3, the pure harmonic oscillator has two essential drawbacks concerning the agreement with experimental single-particle spectra:

(i) A strong spin orbit term must be added in order to reproduce the right magic numbers
(ii) For heavy nuclei, the realistic average potential is rather flat in the interior of the nucleus. Compared to the harmonic oscillator, nucleons at the surface (i.e., nucleons with higher l-values) feel a deeper potential in the realistic case.

In order to include these effects, Nilsson [Ni 55] added two terms to the deformed harmonic oscillator (2.74) and (2.80) and used the Hamiltonian:

$$h = -\frac{\hbar^2}{2m}\Delta + \frac{m}{2}\omega_\perp^2(x^2+y^2) + \frac{m}{2}\omega_z^2 z^2 + C\mathbf{l}\mathbf{s} + D\mathbf{l}^2 \tag{2.89}$$

$$= \hbar\omega_0(\delta)\left(-\frac{1}{2}\Delta' + \frac{1}{2}r'^2 - \beta r'^2 Y_{20}\right) - \kappa\hbar\omega_0(2\mathbf{l}\mathbf{s} + \mu\mathbf{l}^2). \tag{2.90}$$

The constants C and D are given in the form:

$$C = -2\hbar\omega_0\kappa, \qquad D = -\hbar\omega_0\kappa\mu, \tag{2.91}$$

where C gives the strength of the spin orbit force and $D\cdot\mathbf{l}^2$ shifts the levels with higher l-values downward (Fig. 2.20; notice that different μ-values are taken for different shells, as explained below).